Journal of Structural Geology 33 (2011) 1347–1358

Contents lists available at ScienceDirect

Journal of Structural Geology

journal homepage: www.elsevier.com/locate/jsg

Preferred orientation of phyllosilicates: Effects of composition and stress on resedimented mudstone microfabrics

Ruarri J. Day-Stirrat [a,*], Anja M. Schleicher [b], Julia Schneider [c], Peter B. Flemings [c], John T. Germaine [d], Ben A. van der Pluijm [b]

[a] Bureau of Economic Geology, Jackson School of Geosciences, The University of Texas at Austin, University Station, Box X, Austin, TX 78713-8924, USA
[b] Department of Geological Sciences, University of Michigan, C.C. Little Building, 425 E. University Ave., Ann Arbor, MI 48109-1063, USA
[c] Jackson School of Geosciences, The University of Texas at Austin, University Station, C1160 Austin, TX 78712-0254, USA
[d] Massachusetts Institute of Technology, 77 Massachusetts Avenue, Cambridge, MA 02139, USA

ARTICLE INFO

Article history:
Received 23 March 2011
Received in revised form
7 June 2011
Accepted 26 June 2011
Available online 14 July 2011

Keywords:
Preferred orientation
High-resolution X-ray texture goniometry
Resedimentation
Pore-throat size
Boston Blue clay

ABSTRACT

Development of a preferred orientation of clay minerals is investigated in response to changes in vertical effective stress and composition in resedimented material (Boston Blue Clay). Boston Blue Clay (BBC), an illitic glacio-marine clay composed of 57% clay-sized particles (<2 μm) was resedimented and step-loaded to a vertical effective stress of 0.1 MPa, 1 MPa, 6 MPa, and 10 MPa. These four samples show a small increase in preferred orientation of mica and chlorite with increasing vertical effective stress. Furthermore, pure BBC powder was admixed with silica (silt-sized quartz) in five different ratios of BBC:silica to form sediments with 57%, 52%, 48%, 44%, and 36% < 2 μm particles and were loaded to a maximum vertical effective stress of 2.4 MPa. Mica preferred orientation decreases significantly with decreasing clay content at one stress state. We used and compared three different techniques to characterize and quantify the preferred orientation of phyllosilicates: transmission-mode X-ray texture goniometry, reflection-mode X-ray texture goniometry, and grain and pore networks imaged using secondary and backscattered electron micrographs gathered on argon-ion-milled surfaces. Preferred orientation of the clay minerals shows good agreement between transmission-mode X-ray texture goniometry and reflection-mode X-ray texture goniometry. Mercury porosimetry further illuminates vertical effective stress and compositional controls on microfabric.

1. Introduction

Orientation (texture) of clay minerals (phyllosilicates) can be unique to their geological environment of deposition, diagenesis, or deformation. Many studies of preferred orientation of clay minerals that include fault gouge (Solum et al., 2003, 2005; Haines et al., 2009; Solum and van der Pluijm, 2009), low-grade metamorphic rocks (Ho et al., 1995, 1996; Jacob et al., 2000), silt:clay ratios in late diagenesis (Day-Stirrat et al., 2010), and smectite-to-illite transformation (Ho et al., 1999; Day-Stirrat et al., 2008b) provide valuable information regarding sediment-fabric intensity, strain and regional deformation. A detailed understanding of the preferred orientation of clay minerals (phyllosilicates) in mudstones has significant implications for development of permeability anisotropy in shallow burial (Arch and Maltman, 1990), projection of mechanical properties from shallow to greater depth (Ask and Morgan, 2010), and assessment of velocity anisotropy (Domnesteanu et al., 2002). Assessment of the anisotropic properties of fine-grained siliciclastic rocks is becoming more prominent (Sayers, 1994, 1999; Vernik and Landis, 1996; Vernik and Liu, 1997, 2005; Vernik, 2008; Wenk et al., 2008a, 2010; Voltolini et al., 2009). Therefore, a fundamental knowledge of the preferred orientation of clay minerals in these rocks is crucial to understanding the anisotropy of physical properties.

There are several ways to characterize and quantify the preferred orientation of (clay) minerals. Inspection of mica basal planes under an optical microscope (e.g. Sander, 1930) is perhaps the most primitive. Neutron and synchrotron high-energy X-ray diffraction allows access to textures of bulk material and in situ analysis (e.g., Wenk et al., 2008b). Among other X-ray quantitative techniques, the most widely chosen is X-ray diffraction using texture goniometry (e.g. Sintubin, 1994a; van der Pluijm et al., 1994). Image analysis on backscattered electron images has also been used with varying success (e.g. Charpentier et al., 2003; Worden et al., 2005; Fawad et al., 2010).

* Corresponding author. Tel.: +1 512 471 7313.
E-mail address: Ruarri.Day-Stirrat@beg.utexas.edu (R.J. Day-Stirrat).

0191-8141/$ – see front matter © 2011 Elsevier Ltd. All rights reserved.
doi:10.1016/j.jsg.2011.06.007

In this paper, we assess controls on preferred orientation of clay minerals in resedimented materials using three methods, (1) the transmission-mode X-ray technique of van der Pluijm et al. (1994), (2) X-ray reflection-mode preferred orientation (Wenk, 1985; Kocks et al., 1998), and (3) image analysis on argon-ion-milled surfaces subjected to scanning electron microscope imaging. We make links between the evolution of pore-throat size using mercury porosimetry and the preferred orientation of resedimented mudstones. We test two controls on clay-mineral-preferred orientation in resedimented Boston Blue Clay (BBC) and silt mixtures: (1) we use a constant composition and subject the samples to four vertical-effective stress regimes and (2) we vary composition at a constant effective stress by admixing percentages of silt to BBC. Tested samples cover a range of preferred orientations (defined by multiples of a random distribution [m.r.d.]; (Wenk, 1985)), and we demonstrate the variable utility of each technique for quantifying preferred orientation, discuss their robustness, and comment on their applicability. Our study of natural and artificial samples removes the effects of formation condition and compositional heterogeneity and allows us objectively to examine and compare the available methods of clay-mineral-preferred orientation. Resedimentation is used to replicate burial from 10 to 1000 m.

2. Samples and sample preparation

Several samples with variable preferred orientations have been used: BBC, BBC and silt mixtures, kaolinite, and a single-crystal biotite. BBC is an illitic glacio-marine sediment composed of 57% clay-sized particles, <2 μm (Kenney, 1964). The clay-size mineralogy (Table 1) is dominated by 65 wt% illite (mica) and 28 wt% illite-smectite, with lesser amounts of chlorite (5 wt%) and kaolinite (2 wt%). BBC formed the major constituent of our study. We formed two parallel studies on BBC-based materials, in which (1) clay content was constant but vertical effective stress increased and (2) vertical effective stress remained constant and clay content decreased. In both studies, we simulated sedimentation in the laboratory using a method called *resedimentation* (Sheahan, 1991; Santagata and Kang, 2007). In this approach, a sediment slurry is mixed using a particular water content. The slurry is then step-loaded to a stress of 100 kPa in a consolidation device, with water free to leave the system through a filter paper and porous stone. No overpressure is, therefore, maintained. Constant composition samples are loaded to 0.1, 1.0, 6.0, and 10.0 MPa of vertical effective stress, respectively (Table 2). In the constant-stress study, we admixed silica (silt-sized quartz) to dry BBC powder (Table 2) in five different mass ratios of BBC:silica: 100:00, 84:16, 75:25, 68:32, and 50:50. The result was mixtures of clayey-silts and silty-clays with 57%, 52%, 48%, 44% and 36% clay-sized (<2 μm) particles by mass, as determined by hydrometer analyses following ASTM Standard D0422-63R07 (ASTM, 2007). The added silica was 100% quartz with 100% < 64 μm and 10% <2 μm. The admixed BBC and silica were resedimented and consolidated to 100 kPa. The resultant mixtures were further consolidated in a uniaxial constant-rate-of-strain (CRS) device in accordance with the ASTM Standard D4186-06 (ASTM, 2006). Specimens were consolidated at a constant strain rate to a maximum vertical effective stress of 2.4 MPa, which corresponds to a depth of about 250 m under hydrostatic conditions (Schneider et al., in press).

Table 1
Relative percentage of the clay-size fraction of pure BBC.

Relative % of clay minerals in <2-μm clay-size				
Chlorite	Kaolinite	Illite	Illite-smectite	Expandability (%)
5	2	65	28	5

For a pure kaolinite sample (commercially available as EPK Kaolin mined in Florida), we followed the same resedimentation process as for the BBC samples, and we uniaxially consolidated it to 0.1 MPa; it was not subject to CRS testing. We also selected a large single crystal of biotite to represent a crystal endmember in preferred orientation quantification, although it was not resedimented or CRS tested (Table 2).

3. Methods

3.1. High-resolution X-ray texture goniometry

Clay-mineral-preferred orientation was assessed quantitatively using an Enraf-Nonius CAD4 automated, single-crystal diffractometer with a Mo radiation source and a custom-built X-ray pole-figure stage (van der Pluijm et al., 1994). The diffractometer, which measures crystallographic preferred orientation of minerals using the transmission mode, has the advantage of a narrow and high-intensity beam to analyze thick samples while limiting absorption effects. Sample sections cut perpendicular bedding were ground to ~200 μm using fine sandpaper. Samples were analyzed in a two-step process. First, the samples were scanned over a range of 0.5–6.0° 2θ Mo (1–13° 2θ Cu), which indicates the clay-mineral phase present and determines the exact diffraction angles at which textural data should be collected. Second, a "pole-figure scan" (Ho et al., 1995) was performed, in which the degree of preferred orientation of previously identified phyllosilicates was determined. The goniometer and detector were fixed at the diffraction angle, corresponding to the d-spacing of the (001 or 002) reflection of the chosen phase. Samples were then rotated around two axes, one parallel to an imaginary line connecting the goniometer and detector (designated as φ), and one normal to it (designated as ω). Diffracted X-ray-intensity data were collected every 2.5° between 0 and 360° around the φ axis, and in nine steps between 0 and 40° around the ω axis. The X-ray beam was approximately 1 mm^2 at 0° tilt. In total, 1296 intensity measurements were made on each sample. These measurements had to be corrected for X-ray-intensity loss. First, background X-ray intensity was subtracted, then, because X-ray intensity is a tradeoff between absorption (decrease) and irradiated volume (increase) as a function of sample thickness during tilting between 0 and 40°, a correction factor needed to be applied (Fig. 1A). Generation of correction factors is covered in detail in van der Pluijm et al. (1994).

Degree of preferred orientation is obtained from the intensity distribution of diffracted X-rays. Pole-figure diagrams allow visualization of the spatial distribution of X-ray intensities by displaying contour lines representing the pole distribution of (001) phyllosilicate or (002) plane orientations. Plotting pole figures is a quality-control step because the corrections applied to large tilt angles (40°) may be severe. Ideally, in a sample with a high degree of crystallographic preferred orientation, most data should lie between 0 and 25° tilt. Intensity depends on the concentration of crystals aligned parallel to one another. More highly aligned phyllosilicates yield pole figures that are contoured as concentric rings; completely random or isotropic fabrics yield figures that have no poles. Pole density is expressed in m.r.d. (Wenk, 1985), in which higher values reflect higher degrees of crystallographic preferred orientation that can be compared with a growing catalog of similar measurements from a range of settings and depths (e.g. Day-Stirrat et al., 2008b, 2010; Haines et al., 2009).

3.2. Reflection-mode X-ray preferred orientation

Standard reflection-mode goniometry is an alternative technique for quantifying preferred orientation of clay minerals. It can measure average crystallographic orientation of many grains over a sample

Table 2
Samples and physical properties.

Sample	CRS:991 (batch)	CRS:991	BBC_6.0	CRS:991	CRS:046	CRS:047	CRS:048	CRS:050	CRS:051	Kaolinite	Biotite
Clay Content (%)	57	57	57	57	57	52	48	44	36	–	–
Maximum Vertical Effective Stress (MPa)	0.1	1.0	6.0	10.0	2.4	2.4	2.4	2.4	2.4	0.1	–
Equivalent Hydrostatic Depth (m)	10	100	600	1000	240	240	240	240	240	10	–
Void ratio (e)	1.33	0.82	–	0.54	0.67	0.61	0.59	0.56	0.52	1.33	–
Porosity (%)	57	45	–	35	40	38	37	36	34	57	–
Median Pore throat size (nm)	60	52	–	38	64	82	89	105	147	–	–
HRXTG: Mica Preferred Orientation. Maximum pole density (m.r.d.)	4.31, 4.52	4.59	4.83	4.65, 4.49, 4.45	4.86, 4.68	4.12, 3.53, 3.49	3.41, 3.30	4.59, 4.28, 4.01	2.97, 2.81	–	–
XRD: Mica Preferred Orientation (m.r.d.)	–	–	–	–	4.60	4.02, 3.80	3.98,	4.95, 4.84	3.93, 3.91	–	19.70
HRXTG: Chlorite Preferred Orientation. Maximum pole density (m.r.d.)	4.25, 4.02	3.70	4.11	4.27	–	–	–	–	–	–	–
HRXTG/XRD: Kaolinite Preferred Orientation. Maximum pole density (m.r.d.)	–	–	–	–	–	–	–	–	–	1.68/1.91	–

area of tens of square millimeters, while the sample lies flat on a rotating table, making measurement of poorly consolidated or flocculated samples possible. X-ray angular incidence and rotational geometry of the goniometer are explained in Wenk (1985).

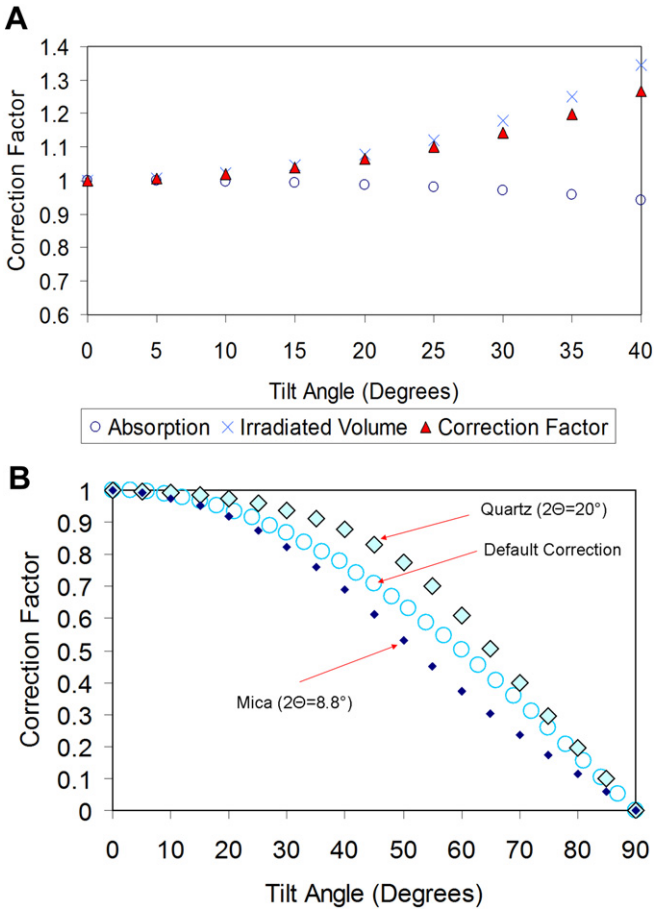

Fig. 1. (A) Absorption, irradiated volume, and associated correction factor for transmission X-ray texture goniometry (HRXTG) of mica in a 0.02-cm-thick sample diffracting at 4.06° 2θ. (B) Defocusing correction factor applied as a function of tilt angle (α) and diffraction angle for mica and quartz in reflection-mode X-ray texture goniometry.

We used reflection-mode X-ray texture goniometry to assess the preferred orientation of mica in resedimented BBC and silt mixtures. The sample was a 2- to 5-mm-thick slab approximately 1.2 cm × 1.8 cm cut perpendicular to bedding and is a parallel cut to that prepared for HRXTG. Since reflection-mode X-ray texture goniometry is highly dependent on the sample surface, care was taken to remove abraded material in sample preparation. We used a Rigaku Ultima IV X-ray diffractometer with cross-beam optics (CBO) and CuKα radiation producing 40 kV and 44 mA. Pole figures were measured using the 3D Explore-Pole Figure software. Our measurement protocol involved detecting the sample height and running a peak scan over 1–13° 2θ for the Cu-anode tube so as to determine the Bragg angle of interest (8.80° 2θ for mica). This diffraction-peak scan also yielded the background X-ray intensity that we subtracted from measured X-ray intensity in quantifying crystallographic preferred orientation. Once the appropriate 2θ angle was determined, the sample underwent X-ray diffraction, following a scanning pattern to cover a pole figure. The scan followed a 3° divergence (α, 0–90°) spaced in 3° azimuth (β, 0–360°) and pole distance. The azimuth rotation (β) was in continuous-scan mode at a speed of 180°/min. Divergence slit, source slit, and receiver slit sizes were 1.0, 2.0, and 2.0 mm, respectively.

Once X-ray intensity was gathered over the whole pole figure (Wenk, 1985), two significant corrections were required. First, background intensity had to be subtracted, which was defined in the initial peak scan over 1–13° 2θ, then X-ray defocusing corrections needed to be applied. In reflection-mode, integrated X-ray intensity remained constant on an infinitely thick sample. Absorption was exactly balanced by irradiated volume increase (Kocks et al., 1998). However, assuming a cylindrical beam, the shape and orientation of an X-ray beam hitting a surface at Bragg angle 2θ and tilt angle α changed for purely geometrical reasons (Kocks et al., 1998). As tilt angle α increases, part of the diffracted beam may fall outside the receiver slit, reducing measured intensity. Ideally a random powder can be prepared and an empirical correction applied to measured intensity. In quantifying crystallographic preferred orientation of clay minerals the 'platy' morphology of clay minerals (e.g. Weaver, 1989) effectively precludes formation of empirical standards. As a result, derived expressions for defocusing effects in clay minerals must be used. There is good agreement between empirical and theoretical curves (Huijser-Gerits and Rieck, 1974) for non-clay diffraction peaks, which define a defocusing correction factor with tilt angle α. For

clay minerals, we require a series of defocusing correction factors that change as a function of 2θ. Assuming a Gaussian intensity distribution of the Bragg peak, Gale and Griffiths (1960) and Tenckhoff (1970) produced ratios of intensity ($I_\alpha/I_{\alpha=0^\circ}$) before and after tilting. Various forms of this derived expression (presented graphically in Fig. 1B) can be found in Gale and Griffiths (1960), Huijser-Gerits and Rieck (1974), and most accessibly in Kocks et al. (1998, page 146). Fig. 1B aptly describes the potentially severe effects of defocusing in reflection-mode X-ray texture goniometry; as a result, a pole figure can be measured reliably only to tilt angles (α) 80°–85° (Kocks et al., 1998). We therefore chose to cut our data at $\alpha = 81^\circ$ (we increased α at 3° steps). Similar to HRXTG, pole density is again expressed in m.r.d. (Wenk, 1985), allowing for direct comparison of fabric intensities.

3.3. Imaging

Secondary electron microscopy (SE) images of pores and pore networks, as well as backscattered electron microscopy (BSE) images of grain morphology and location, were collected on argon-ion-milled surfaces on select samples from BBC and silica sample sets. The nonlithified nature of the samples precluded conventional thin-section cutting and polishing because of plucking of the sample surface by the grinding abrasive. As a result, we used argon-ion milling to produce surfaces cut perpendicular to bedding (lamination) that show only minor topographic relief unrelated to differences in mineral hardness. The argon-ion-milling system was operated at an accelerating voltage of 5–7 kV and a gun current of approximately 300 μA. These settings have proved effective in producing relatively flat surfaces for imaging pores (Loucks et al., 2009). Samples were examined using a Zeiss Supra 40 VP field-emission Scanning Electron Microscopy, with SE and BSE detectors using an accelerating voltage of 10 kV, a spot size of 3.0, and a working distance of approximately 5 mm.

Using the BSE images captured on argon-ion-milled surfaces, we recorded three pieces of data for two samples (CRS46 and CRS51) concerning clay minerals in JMicrovision (Roduit, 2008) line length, line orientation, and line azimuth. Line orientation is defined as the angle between the horizontal axis (arbitrarily the base of the image) and the line (0–180° counterclockwise) and line azimuth as the horizonal angular distance from the north point of the line made clockwise through 360° by placing the center of the circle on the first point of the line.

3.4. Pore-throat size

Pore-throat size distributions, through mercury porosimetry (MICP), were determined on a 1-g block of sample that was freeze dried (Delage and Lefebvre, 1984) for 24 h, then dried in an oven at 105 °C for another 24 h. Porosities were calculated from dry bulk density (ρ_d) and grain density (G_s):

$$\phi = 1 - \frac{\rho_d}{G_s} \tag{1}$$

Grain density was measured on samples dried at 105 °C using the Small Pyknometer Method. Dry bulk density was calculated from the bulk volume of the known mass of sample in the process of measurement of pore-throat size distribution using the mercury intrusion technique. Pore-throat size distributions were determined on a *Micromeritics*© Autopore Π 9220. Pore-throat sizes were calculated from the mercury intrusion data. The analysis worked on the assumption that the surface tension of mercury was 0.48 N/m and the contact angle between mercury and the particle surface was 141°. Pore radius, *r*, is given by

$$r = 746000 \Big/ p \tag{2}$$

where *r* is the pore-throat radius (nm) and *p* is pressure in kPa.

4. Results

4.1. Crystallographic preferred orientation

4.1.1. Clay-mineral-preferred orientation from high-resolution X-ray texture goniometry

In high-resolution X-ray texture goniometry, we record the preferred orientation (maximum pole density in m.r.d.) of mica and chlorite in resedimented BBC consolidated to 0.1, 1.0, 6.0, and 10.0 MPa of vertical effective stress. Chlorite preferred orientation is systematically lower than mica preferred orientation by about 0.5 m.r.d. (Fig. 2). Both phases show a small increase in preferred orientation with increasing vertical effective stress (Table 2, Fig. 2). Mica preferred orientation in the sample at 6 MPa appears slightly off the overall trend, which could result from sample preparation, internal sample heterogeneity, or localized crystallographic effects.

BBC and silica samples at constant vertical effective stress show a general decrease in mica preferred orientation with decreasing clay content (Fig. 3). Data quality is high, given recorded lower-hemisphere-equal-area projections for each sample. The sample at 44% clay-sized material has an anomalously high mica preferred orientation, but repeated analyses of different areas of this sample found comparable results. The kaolinite sample [(001) basal peak] compressed to 0.1 MPa recorded an m.r.d. of 1.68, with multiple poles recorded on lower-hemisphere-equal-area projection (Fig. 4). We did not analyze the biotite sample by HRXTG because of preparation difficulties.

4.1.2. Clay-mineral preferred orientation from reflection-mode X-ray texture goniometry

In reflection-mode X-ray texture goniometry, the trend in mica preferred orientation (maximum pole density) is similar to that in the HRXTG samples of varying clay-size fraction at constant vertical effective stress (Fig. 3C and Table 2). The high preferred orientation in the 44% clay-sized sample in HRXTG can be replicated in reflection-mode scanning. Also, the stereographical representation of data for the 57% clay-sized samples shows a similar pattern, although in HRXTG we plot iso-contours of m.r.d. values and in X-ray reflection we plot iso-contours of X-ray intensity (m.r.d. is directly derived from X-ray intensity and is simply weighed with respect to its areal distribution). The sample with 36% clay-sized

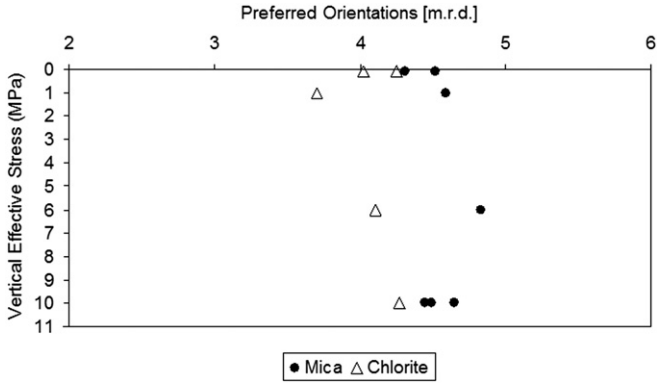

Fig. 2. Resedimented Boston Blue Clay (BBC) with 57% clay-size particles by mass shows a small increase in preferred orientation (maximum pole density) with increasing vertical effective stress over a range of 0.1–10 MPa for both mica and chlorite. Data collected by HRXTG.

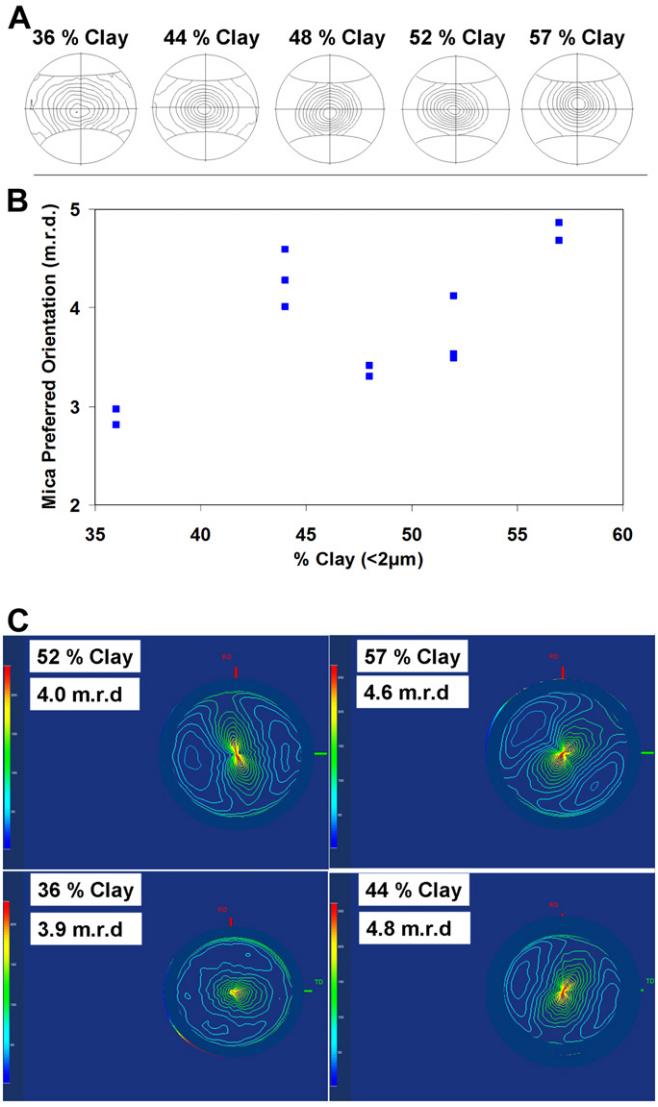

Fig. 3. (A) Pole figures for BBC admixed with silica (silt-sized quartz) showing iso-contours of m.r.d. values (contour interval varies). (B) Percentage clay and mica preferred orientation (maximum pole density) at a constant vertical effective stress of 2.4 MPa. Data collected by HRXTG. (C) Pole figures of reflection-mode X-ray texture goniometry data showing iso-contours of X-ray intensity. Preferred orientation of mica quoted in multiples of a random distribution (m.r.d.).

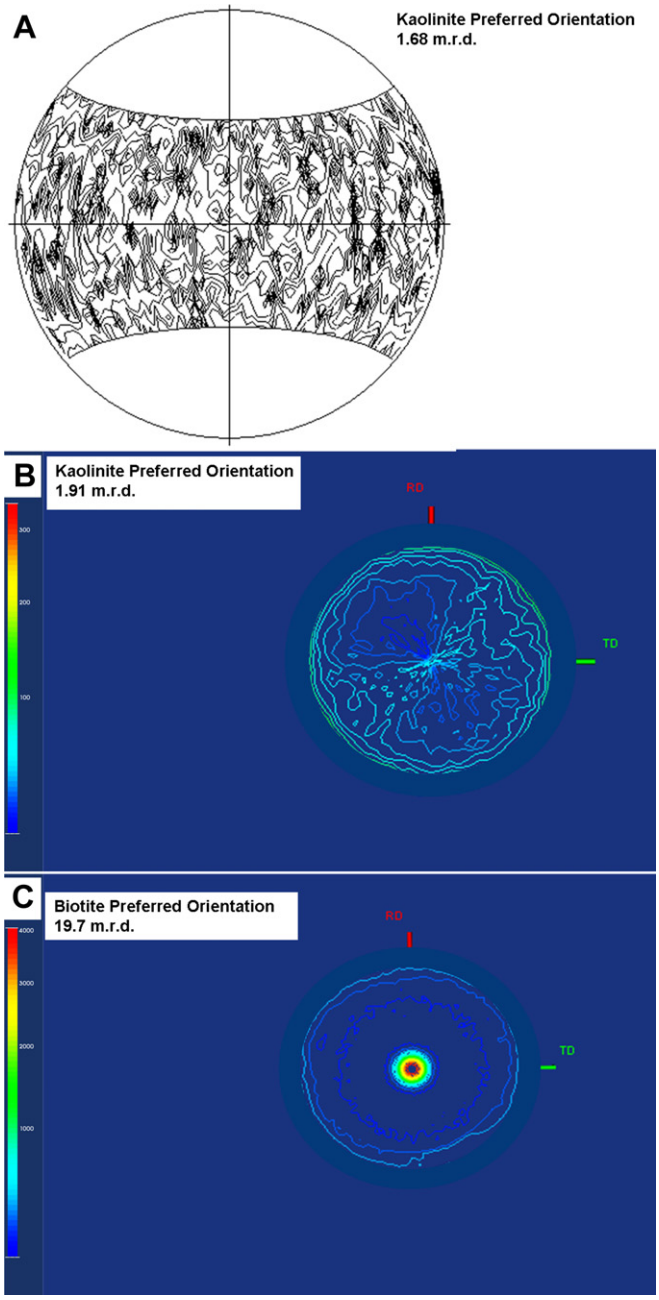

Fig. 4. (A) Kaolinite at 0.1 MPa vertical effective stress has a maximum pole density of 1.68 m.r.d. using HRXTG. (B) Kaolinite at 0.1 MPa vertical effective stress in reflection geometry has an m.r.d. of 1.91. (C) A single-crystal biotite has a strong preferred orientation (19.7 m.r.d.).

material in reflection geometry recorded a slightly higher mica preferred orientation than in HRXTG. This difference most likely resulted from our preparation technique, in which, as we ground the sample to the correct height for analysis, we may have emplaced abraded material (mica) into the large pores of the sample. We thus recorded a higher mica preferred orientation.

In reflection-mode X-ray texture goniometry, the preferred orientation of kaolinite was found to be 1.91 m.r.d. For this sample, there was close agreement between reflection and transmission (HRXTG) modes. The single-crystal biotite recorded an m.r.d of 19.7 in reflection-mode (Fig. 4).

4.2. Imaging

4.2.1. Pore imaging

In BBC samples admixed with varying silt fractions (silica) at a constant vertical effective stress, we document generally angular pore shapes that increase in size with increasing silt fraction (Fig. 5).

When we present matching pairs of secondary images and back-scattered images (Fig. 5B, D, F) we are able to discern the compositional effect on pore size. The largest pores are associated with the boundary of silt particles. Clay-sized material contains pores that are orders of magnitude smaller than pores associated with silt particles. Pore images show that the high-silt-content sample (Fig. 5E, F) has a broad range of pore sizes, whereas the sample with the least silt has a much narrower range of pore sizes (Fig. 5A, B).

4.2.2. Clay-mineral preferred orientation in images

4.2.2.1. Line orientation. The angle between the horizontal axis (arbitrarily the base of the image) and the measured line of quantified length for two representative images at the same

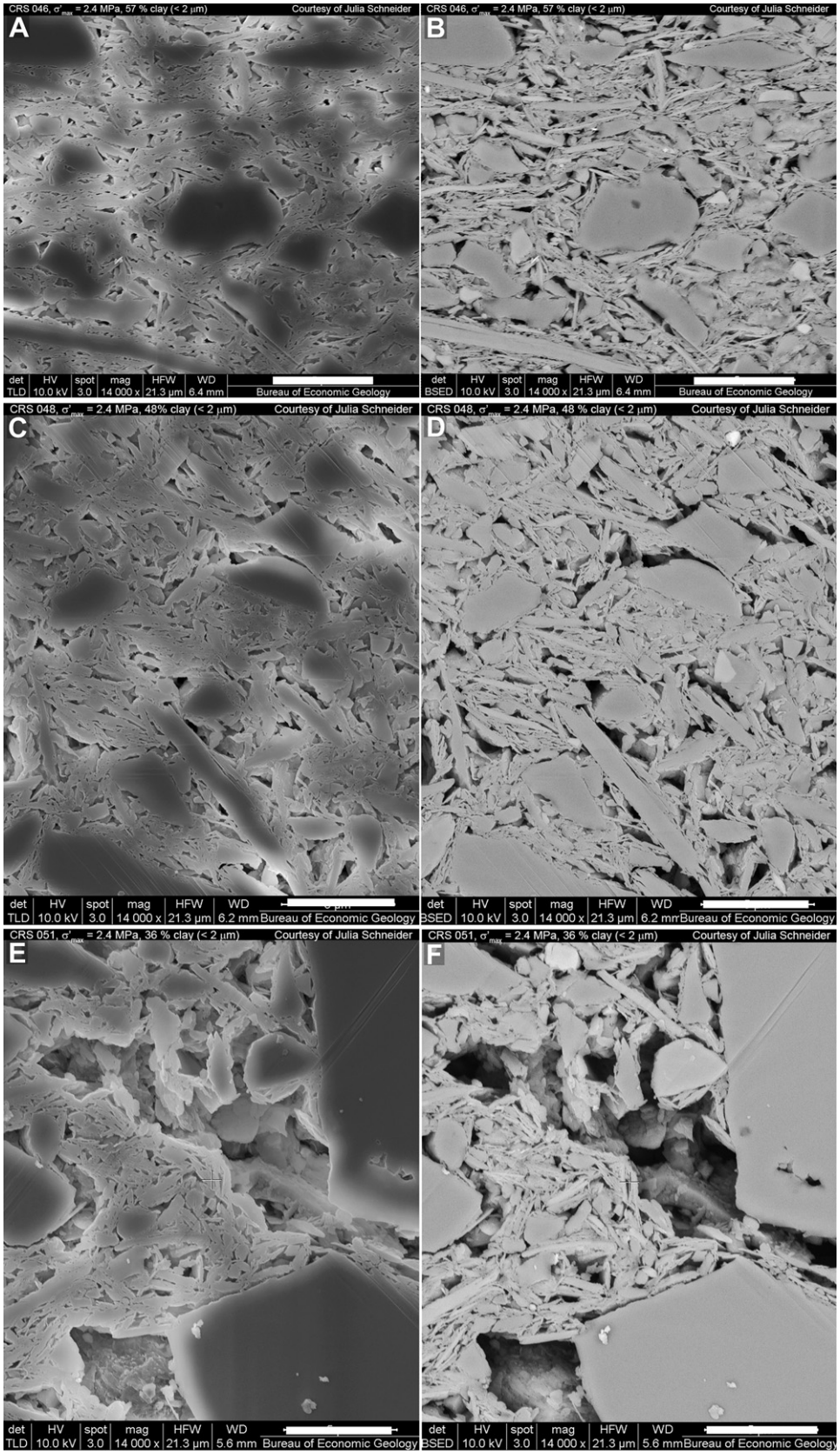

Fig. 5. Left column comprises secondary electron images of pores and pore throats. Right column shows backscattered electron images. Images are produced on a flat argon-ion milled surface. (A and B) CRS:046, 57% clay. (C and D) CRS:048, 48% clay. (E and F) CRS:051, 36% clay. Scale bar 5 μm.

magnification for two samples (CRS:046 and CRS:051; see Table 2) were analyzed. Samples CRS:046 and CRS:051 have 486 and 523 line observations, respectively. Results show line length to average about 1 μm and to be concentrated at 0–40° and 140–180° for CRS:046 (Fig. 6). Sample CRS:051 has a uniform distribution of line orientations from the horizontal. Visual confirmation of this phenomenon can be found in BSE images. CRS:046 has more clay minerals oriented approximately parallel to the base of the image than does CRS:051. We chose not to create rose diagrams common in structural geology (e.g. Manda et al., 2008) because of the mostly qualitative nature of our data.

4.2.2.2. Line azimuth. Line azimuth, the horizontal angular distance from the north point on a line made clockwise through 360°, has two distinct groups of azimuth data for CRS:046 (57% clay). One group of azimuth data is angled between 60 and 120°,

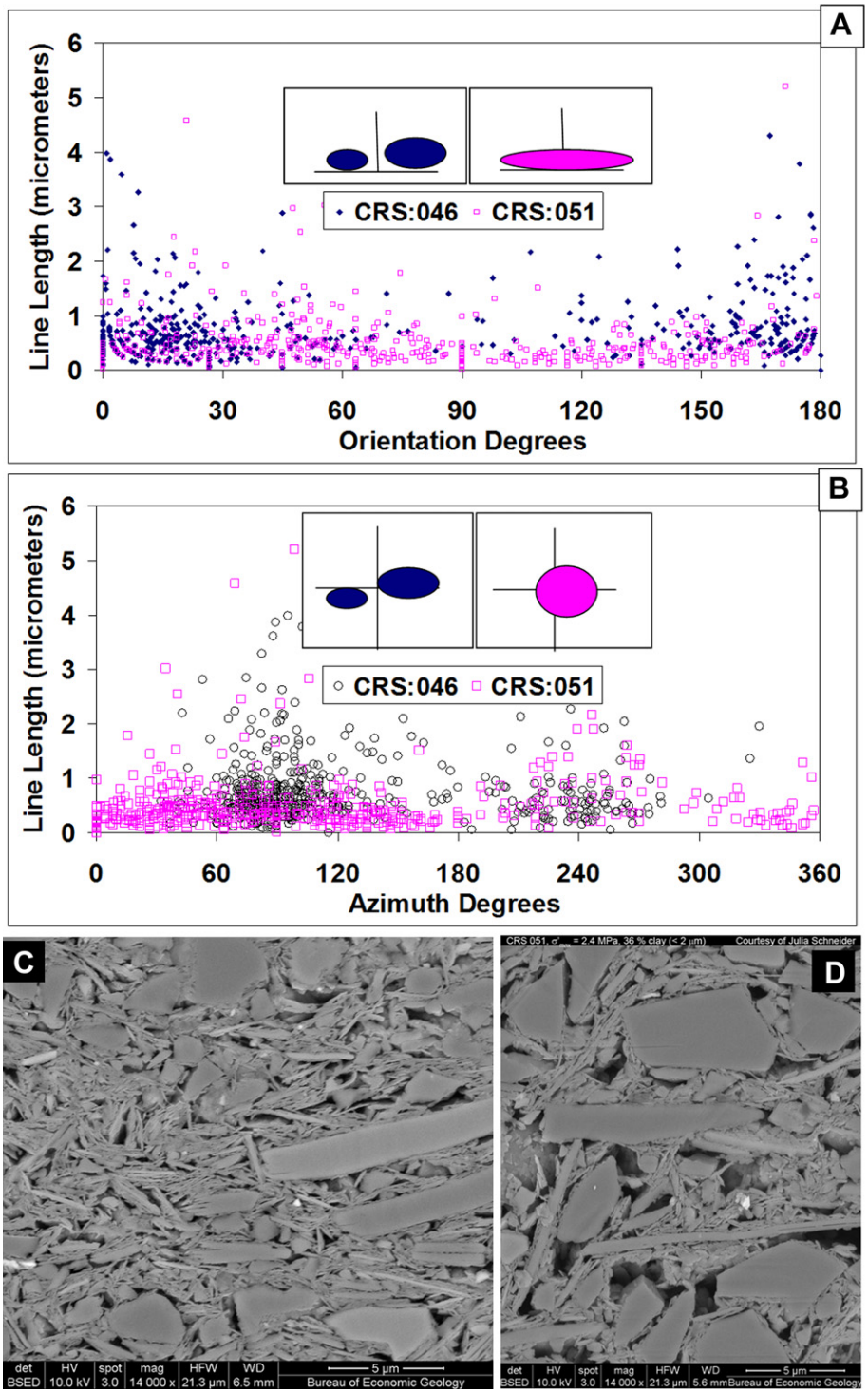

Fig. 6. (A) Orientation angle and line length of clay particles. (B) Azimuth and line length and BSE images of CRS:046. (C) Sample has 57% clay-sized particles and CRS:051. (D) Sample has 36% clay-sized particles prepared on an argon-ion milled thin section. Inset boxes in A and B show qualitative orientations of preferred clay mineral alignment.

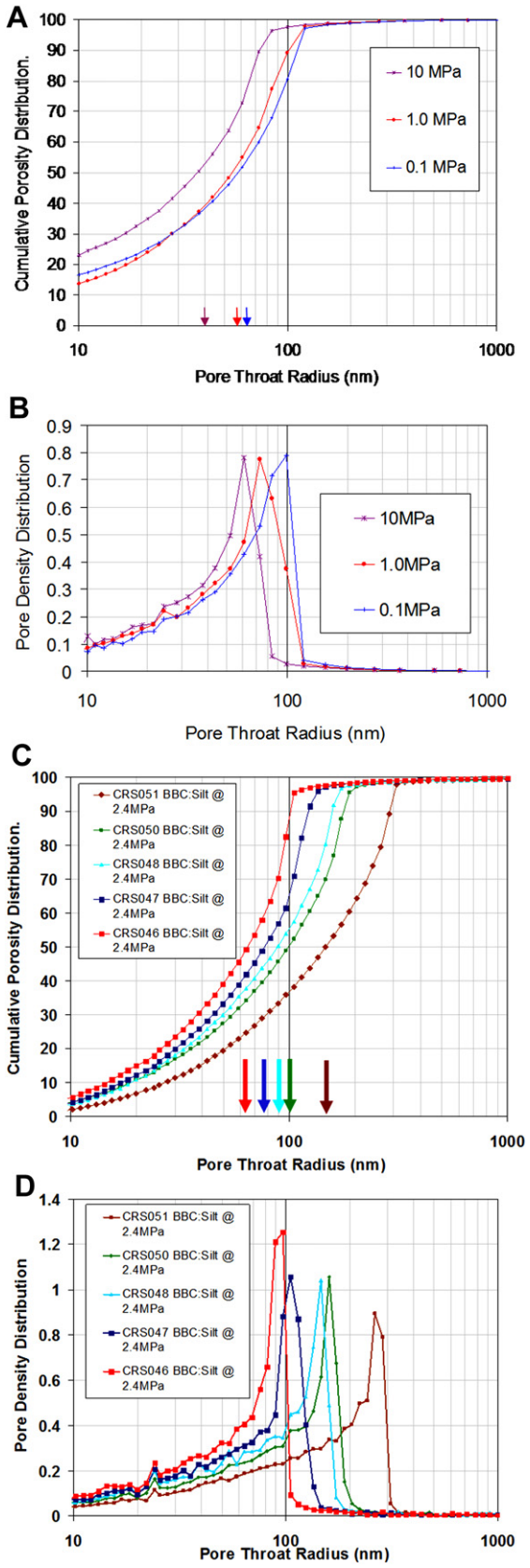

Fig. 7. (A and B) Three different vertical effective stress states, 0.1, 1.0, and 10.0 MPa of resedimented BBC, 57% clay. (A) Median pore-throat size (arrows) decrease for 0.1, 1.0, and 10.0 MPa vertical-effective-stress ranges. (B) Pore-density distributions decrease in modal pore-throat size (peak of distribution), and there is a general decrease in pore-throat size. (C and D) Resedimented BBC and silt at constant vertical effective stress (2.4 MPa). (C) Adding silt to BBC increases pore-throat size (arrows). (D) Modal pore-throat size shifts to larger pore-throat sizes with silt addition, and overall pore-density distribution is dominated by larger pore-throat sizes.

and the other between 200 and 270° (Fig. 6). CRS:051 has a more even distribution of line lengths over a full azimuth. According to the BSE image, these semi-quantitative descriptions of clay mineral orientations CRS:046 and CRS:051 have differently oriented clay particles, in agreement with X-ray quantifications.

4.3. Pore-throat size distributions

In resedimented BBC (57% clay) loaded to three different vertical effective stresses, we observe a systematic decrease in median pore-throat size (Fig. 7a) with increasing vertical effective stress. The highest vertical effective stress sample (10 MPa) has a pore-throat size curve that appears as a simple translation of lower vertical effective stress curves. An overall reduction in porosity (Table 2) is related to loss of the largest pores, and by examining pore-density distributions (Fig. 7b), we find this reduction to be reasonable. Shapes of distributions are almost identical, yet the modal point (peak of distribution) shifts to lower pore-throat sizes with increasing vertical effective stress.

At constant stress and by varying clay content, we note a significantly different behavior. With increasing silt content, the median pore-throat size shifts to higher values (Fig. 7c) systematically. The pore-density distributions of these mixtures (Fig. 7d) show a marked contrast to those of the constant composition samples. The modal point shifts to larger pore-throat sizes with increasing silt, and it has a lower density peak. This behavior describes a distribution that is dominated increasingly by larger pores, which are fewer in number. The areas under each curve are approximately equal (Table 2) and equate to total porosity.

5. Discussion

5.1. Resedimentation and parameter testing

Owing to homogeneity, absence of sample disturbance, and the ability to control stress history, resedimentation allows the systematic testing of samples in which one parameter changes at a time. Our sample sets, which consist of BBC at four different stress regimes and BBC mixed with silt in differing ratios at one-stress state, were created to carefully study vertical effective stress and compositional controls on preferred orientation of clay minerals in shallow burial (<1 km). We observe two distinct behaviors controlled by stress and composition. First, preferred orientation of mica increases with increasing vertical effective stress, and concomitantly we note a decrease in total porosity and median pore-throat size. Second, at constant vertical effective stress, compositional changes—specifically the silt:clay ratio—systematically decrease preferred orientation of mica with increasing silt content and increase median pore-throat size, whereas total porosity remains approximately constant.

5.2. Choice of technique for preferred orientation

For cases in which a sample can be easily prepared into a thin section, HRXTG has historically been well suited (Sintubin, 1994a, b; van der Pluijm et al., 1994; Ho et al., 1995, 1996, 1999; Jacob et al., 2000; Aplin et al., 2006; Day-Stirrat et al., 2008a, 2008b; Debacker et al., 2009; Haines et al., 2009; Solum and van der Pluijm, 2009; Day-Stirrat et al., 2010). Relatively minor corrections (van der Pluijm et al., 1994) and the possibility to make orthogonal cuts

allowing a complete pole figure to be generated (Debacker et al., 2009) make HRXTG an attractive way of quantifying clay-mineral preferred orientation. The relatively small sample-interaction volume (~1-mm diameter of 0.2-mm-thick sample) of HRXTG makes clay-rich fault gouges particularly suitable for study (e.g. Haines et al., 2009; Solum and van der Pluijm, 2009). Major drawbacks also exist, however. First, in transmission-mode, a sample is mounted onto a holder, which represents a problem for poorly consolidated material and powders. Second, low X-ray scattering power, structural disorder, and the coexistence of phases (e.g., 001 kaolinite and 002 chlorite at 5.80° 2θ using a Mo-source) create peak broadening as tilt (α) and rotation (β) increase. The technique has generated hundreds of reliable analyses and is a relatively fast process—around 6 h for complete sample preparation, phase identification, and quantification of two mineral peaks.

Quantifying preferred orientations of clay minerals using reflection-mode X-ray texture goniometry is an underutilized technique that results principally from large corrections at high tilt angles (Fig. 1A) and the low scattering efficiency of most Cu-anode X-ray devices. However, we find good agreement between transmission and reflection geometries for strongly crystalline clay minerals like mica (Fig. 3), kaolinite (Fig. 4 and Table 2), and single-crystal biotite. Beyond the noted drawback surrounding high correction factors, principal drawbacks are broadly the same as for HRXTG—namely, low X-ray scattering power, structural disorder of phases, and coexistence of phases, although each is magnified by both the lower intensity of the Cu-anode relative to the Mo-anode and the correction factor. Because the sample rests on a flat surface, we can measure flocced clays or poorly consolidated samples, which is more difficult in HRXTG. Further, the good agreement between kaolinite with a low preferred orientation indicates this future utility. Finally, sample run times are shorter than for HRXTG (~1 h).

Synchrotron-generated hard X rays were not available in this study; however, their utility, combined with Rietveld analysis (Wenk et al., 2008a, 2008b; Lutterotti et al., 2009; Voltolini et al., 2009; Wenk et al., 2010) in quantifying crystallographic preferred orientation, shows considerable promise in the following areas. Samples with a low preferred orientation can be measured with great accuracy, overlapping peaks can be deconvoluted, and the different preferred orientation of illite-smectite and illite can be assessed on the same broad peak. The range of clay-mineral preferred-orientation quantifications using synchrotron-generated hard X-rays (Wenk et al., 2008a, 2008b; Lutterotti et al., 2009; Voltolini et al., 2009; Wenk et al., 2010) are broadly in agreement with HRXTG-based studies (e.g.van der Pluijm et al., 1994; Ho et al., 1995, 1996, 1999; Jacob et al., 2000; Aplin et al., 2006; Day-Stirrat et al., 2008a, 2008b; Haines et al., 2009; Solum and van der Pluijm, 2009; Day-Stirrat et al., 2010). The main issues with the technique are access to a hard X-ray source and the complex and time-consuming nature (potentially days) of Rietveld refinement.

Backscattered electron images are typically used in studies of preferred orientation to qualitatively assess the data gathered through X-ray techniques (Aplin et al., 2003, 2006; Day-Stirrat et al., 2008a, 2008b, 2010). Conventional thin-section preparation often plucks the smallest particles from a thin section, yet it is these images on which microfabric has been assessed. Image-analysis techniques to quantify microfabric rely on dealing with a pixel that represents a part of a larger grain and on its relationship to other particles. This process is challenged with image analysis issues in which subjective, user-defined, pixel-intensity cutoffs are made to select a density window to optimize grain separation (Worden et al., 2005). From these processes, an anisotropy ratio (Charpentier et al., 2003; Worden et al., 2005) is developed, ranging from 1 in a sandstone to approximately 25 in a metamorphic pelite. Grain sizes below a certain limit will tend to become rounded, exhibiting an aspect ratio of 1 (Fawad et al., 2010) or an anisotropy ratio of 1 (Worden et al., 2005).

We recognize the difficulty of using BSE images to assess clay-mineral preferred orientation quantitatively. X-ray techniques are used to measure the orientation and intensity of the basal reflection of a clay mineral for a predetermined phase, which occurs passively because differently oriented phases diffract at different tilt (α) and rotation angles (β). Image-analysis techniques require a viewer to make subjective decisions on the orientation of a clay mineral. Lines A through D (Fig. 8) point to four <1-μm clay minerals, each in a different orientation. In two instances (A and C), the A- or B-axis of the clay is observed (basal planes) perpendicular to the plane of the image, and a line can be drawn that has a length orientation to the horizontal and an azimuth. Two other clay minerals (B and D) are imaged at some oblique angle to the plane of the image so that we may observe the clay particle down C-axis. In an X-ray technique, these latter two clay-mineral particles would not diffract in this geometry, although in image analysis a viewer must decide where to draw a line and record length, orientation, and azimuth. Given these issues, we include our high-quality BSE images only as qualitative to semiquantative descriptions of clay-mineral preferred orientation.

5.3. *Vertical effective stress control on crystallographic preferred orientation*

We obtained preferred orientations of mica over a vertical-effective-stress range of 0.1–10.0 MPa that are higher (~4.5 m.r.d.) than those of a low-stress study (Haines et al., 2009), in which crystallographic preferred orientations of montmorillonite were low (1.6–1.8 m.r.d.). However, our results are comparable to those of a recent study (Voltolini et al., 2009) using synchrotron-generated hard X rays and Rietveld analysis. These workers took varying mixtures of clay (25% illite, 75% kaolinite) and quartz and subjected them to uniaxial effective stresses (no lateral strain). The 100% clay sample consolidated to 5 MPa produced crystallographic preferred orientations of 5.26 and 4.11 m.r.d. for

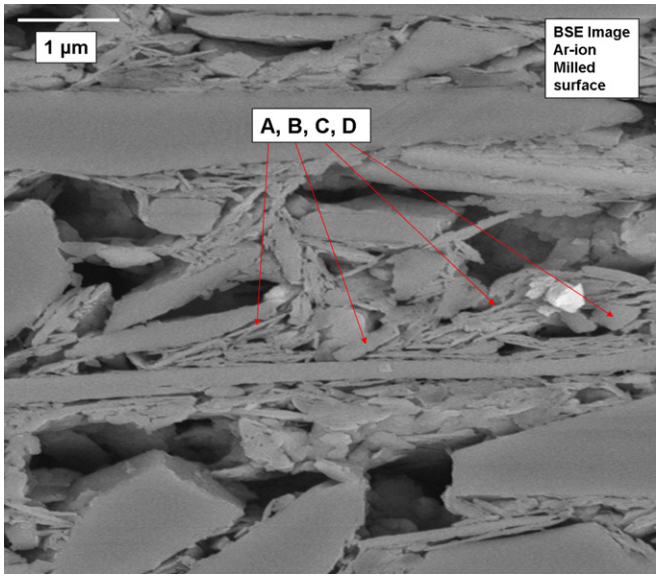

Fig. 8. Lines A, B, C, and D point to approximately equal-sized clay minerals in differing orientations. Sample is CRS:051 (36% clay-sized particles by mass).

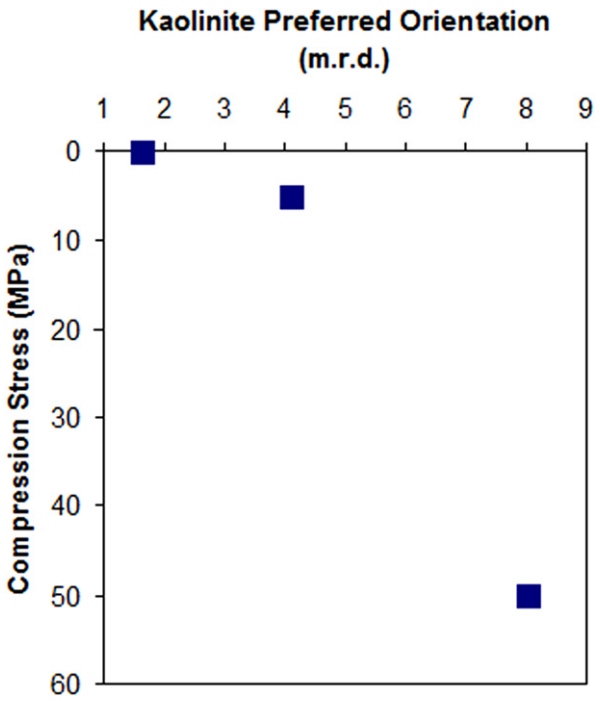

Fig. 9. Kaolinite preferred orientation (maximum pole density in m.r.d.). Our sample at 0.1 MPa vertical effective stress is combined with data from Voltolini et al. (2009), 5 and 50 MPa of compressive stress.

illite and kaolinite, respectively. Their 50% clay and 50% silt produced crystallographic preferred orientations of 1.7 m.r.d. for both and kaolinite at 5-MPa consolidation (taken to equate to ~500 m of burial), and, hence, percent quartz dominates fabric-intensity development.

The 100% montmorillonite samples of Haines et al. (2009), loaded to 10, 50, and 150 MPa, produced only weak fabric intensities (1.6–1.8 m.r.d.). Shearing these consolidated samples produced stronger crystallographic preferred orientations (1.7–4.6 m.r.d.), and crystallographic preferred orientation increased with increasing shear strain.

Under uniaxial consolidation conditions, differences in clay mineralogy (Voltolini et al., 2009) will influence the maximum crystallographic preferred orientation that a sample may produce because of the wavy nature of montmorillonite basal planes (Schleicher et al., 2009). Our crystallographic preferred orientations of mica suggest that the crystallinity of this mineral heavily influences maximum pole density (m.r.d.). If we compare our quantification of preferred orientation of mica at 10 MPa of vertical effective stress (Fig. 2) with the montmorillonite sample of Haines et al. (2009) at 10 MPa, we can document this effect, in which our quantifications of preferred orientation are more than 2 m.r.d. higher at the same stress. The studies differ in that the role of fluids facilitating clay-mineral preferred orientation were not rigorously assessed (Haines et al., 2009 experiments were run dry), and it has been suggested that lubricating fluids may influence clay-mineral preferred orientation (Day-Stirrat et al., 2008a). A variety of studies both in the lab (Haines et al., 2009; Voltolini et al., 2009) and on in situ samples (Ho et al., 1999; Aplin et al., 2006; Day-Stirrat et al., 2008a) at low vertical effective stress and approximately comparable clay contents point to a progression in preferred orientation governed by crystallinity. Smectite (montmorillonite) always has a low preferred orientation, and mica a preferred orientation higher than smectite. Chlorite has a crystallographic preferred orientation lower than that of mica, which is, in turn, higher than that of mixed layer-phase illite-smectite (compare with shallow samples in Ho et al., 1999; Day-Stirrat et al., 2008a). Where kaolinite sits in this trend of smectite, illite-smectite, chlorite, and mica at one stress state is not entirely clear. We combine our data (Fig. 9) with the 100% clay sample from Voltolini et al. (2009) and show a significant change in preferred orientation over 0.1–5 MPa (Fig. 9). Our data suggest that at low vertical effective stress, kaolinite has a preferred orientation similar to that of smectite but at higher stresses (Voltolini et al., 2009) kaolinite is comparable to chlorite (compare Figs. 3 and 9). Further study on the effects of stress state on kaolinite is required to resolve these differences.

Over a stress range of 0.1–10 MPa, vertical effective stress exerts a small control over phyllosilicate-preferred orientation (Fig. 2).

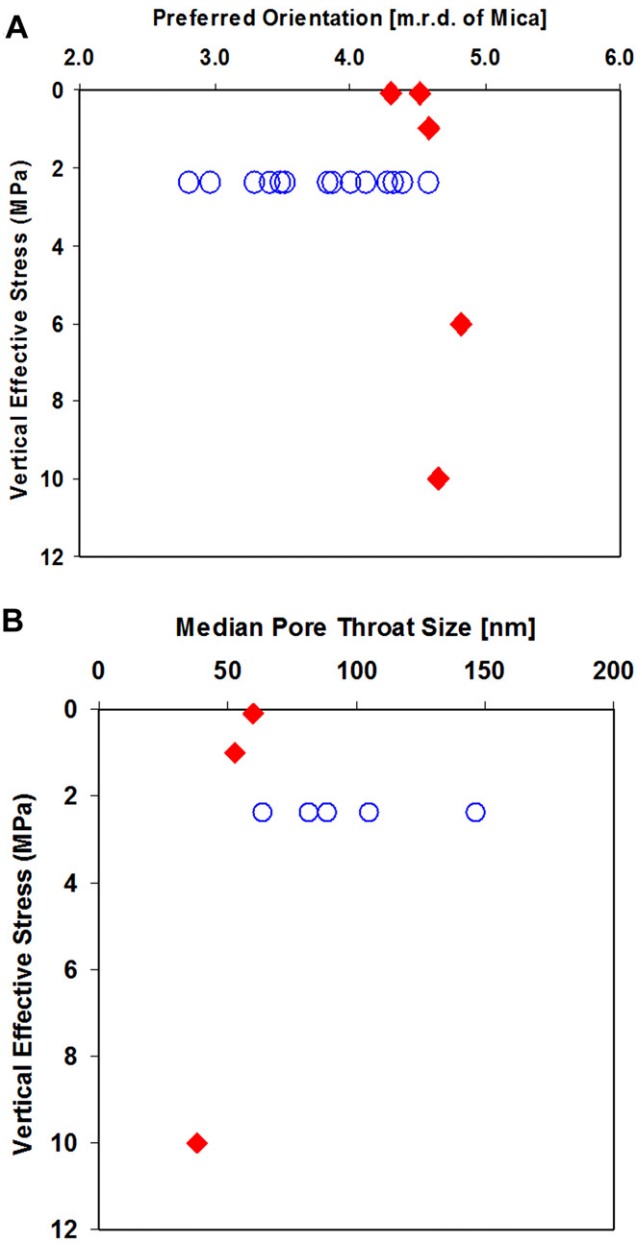

Fig. 10. (A) Mica preferred orientation (maximum pole density) in HRXTG as a function of vertical effective stress for both constant composition (solid symbols) and varying silt (open symbols) component BBC samples. (B) Median pore-throat size as a function of vertical effective stress for both constant composition and varying silt component BBC samples.

This stress control is true for both chlorite and mica, in which small increases in preferred orientation are recorded. We conclude that passive rotation of particles into a microfabric that is dominated by grains aligned perpendicular to loading in response to pore closure is only a minor mechanism in the development of a clay-mineral-preferred microfabric.

5.4. Compositional control on clay-mineral preferred orientation

Resedimented BBC and silt mixtures show a strong compositional effect on the preferred orientation of mica. Increasing silt content at constant vertical effective stress (2.4 MPa) reduces mica preferred orientation from a high of 4.9 m.r.d. to a low of 2.8 m.r.d., as total clay decreases from 57% to 36% (Table 2, Fig. 3). The shape of this mica preferred orientation decrease with increasing silt content has the same trend as that of illite and silt, which was quantified by Voltolini et al. (2009, see their Table 2) at 5 MPa. Our data, however, have a much sharper preferred-orientation decline over a smaller clay-content range. These results suggest that clay content has a bigger influence over preferred orientation than stress alone. Image analysis of our endmember clay-content examples, 57% and 36% clay, shows the effects of silt content on maintaining large pores (Figs. 8 and 10). Our samples make a transition from a matrix-supported microfabric (Fig. 5b) to a grain-supported microfabric (Fig. 5F). Grain-supported microfabric effects have significant control over fluid flow (Schneider et al., in press) and in deeper parts of sedimentary basins control the maximum preferred orientation that a mineral phase may achieve through diagenesis (Day-Stirrat et al., 2010).

5.5. Whole-rock fabric and anisotropy

Vertical effective stress and composition demonstrably change clay-mineral preferred orientation and have implications for the microfabric of the soil in question. Using BSE images, we can qualitatively show microfabric evolution with changes in the silt:clay ratio (Fig. 5). A further step is to use mercury porosimetry data to upscale the discussion of microfabric from approximately 400 μm^2 (the area of our images) to 1 cm^3. As with phyllosilicate-preferred orientation, vertical effective stress has a small effect on median pore-throat size in samples of the same composition relative to samples of varying clay content. As a result, we gain insight into microfabric behavior on the basis of stress and composition (Fig. 10). Although recognition of porosity loss or reduction in median pore-throat size is not new, our study offers the context for a picture of microfabric that is dynamic on the basis of composition and vertical effective stress, in which we are able to demonstrate that composition is the dominant control on mica preferred orientation. Our results, therefore, have important implications for the way heterogeneity is viewed. At similar stresses, small changes in composition can have significant impact on the microfabric of a rock. These changes affect permeability, mechanical response, electric properties, and how pores are filled by diagenetic phases.

6. Conclusion

We use three techniques to assess the preferred orientation of phyllosilicates in resedimented materials. We found good agreement in preferred-orientation quantification between transmission-mode X-ray texture goniometry and reflection-mode X-ray texture goniometry analyses for clays in resedimented BBC samples and resedimented kaolinite. Our study shows that in resedimented material, an increase in vertical effective stress exerts a small control over mica and chlorite preferred orientation and median pore-throat size but that silt:clay ratios have a greater control on both. Backscattered electron images, in contrast, are able to qualitatively describe only the silt matrix control on preferred orientation and porosity at higher silt contents.

Acknowledgments

We thank UT Geofluids Industrial Associates Program for its sponsorship. HRXTG and XRD are supported by Electron Microbeam Analysis Laboratory (EMAL) at the University of Michigan and NSF grant EAR-0345985 to Ben van der Pluijm. Mark Andrews and Carl Henderson are thanked for assistance in the lab; Robert M. Reed prepared BSE images. Publication authorized by the Director, Bureau of Economic Geology. Reviews by John G. Solum and Kyu Kanagawa were greatly appreciated.

References

Aplin, A.C., Matenaar, I.F., McCarty, D.K., van der Pluijm, B.A., 2006. Influence of mechanical compaction and clay mineral diagenesis on the microfabric and pore-scale properties of deep-water Gulf of Mexico mudstones. Clays and Clay Minerals 54, 500–514.

Aplin, A.C., Matenaar, I.F., van der Pluijm, B., 2003. Influence of mechanical compaction and chemical diagenesis on the microfabric and fluid flow properties of Gulf of Mexico mudstones. Journal of Geochemical Exploration 78-9, 449–451.

Arch, J., Maltman, A., 1990. Anisotropic permeability and tortuosity in deformed wet sediments. Journal of Geophysical Research 95, 9035–9045.

Ask, M.V.S., Morgan, J.K., 2010. Projection of mechanical properties from shallow to greater depths seaward of the Nankai accretionary prism. Tectonophysics 482, 50–64.

ASTM, 2006. Standard test method for one-dimensional consolidation properties of saturated cohesive soils using controlled-strain loading (Standard D 4186-06). In: International, A. D 4186-06, West Conshohocken, PA, p. 15.

ASTM, 2007. Standard test method for particle-size analysis of soils. In: International, A. D 422-63, West Conshohocken, PA, p. 8.

Charpentier, D., Worden, R.H., Dillon, C.G., Aplin, A.C., 2003. Fabric development and the smectite to illite transition in Gulf of Mexico mudstones: an image analysis approach. Journal of Geochemical Exploration 78-79, 459–463.

Day-Stirrat, R.J., Aplin, A.C., Srodon, J., van der Pluijm, B.A., 2008a. Diagenetic reorientation of phyllosilicate minerals in Paleogene mudstones of the Podhale Basin, southern Poland. Clays and Clay Minerals 56, 100–111.

Day-Stirrat, R.J., Dutton, S.P., Milliken, K.L., Loucks, R.G., Aplin, A.C., Hillier, S., van der Pluijm, B.A., 2010. Fabric anisotropy induced by primary depositional variations in the silt: clay ratio in two fine-grained slope fan complexes: Texas Gulf Coast and northern North Sea. Sedimentary Geology 226, 42–53.

Day-Stirrat, R.J., Loucks, R.G., Milliken, K.L., Hillier, S., van der Pluijm, B.A., 2008b. Phyllosilicate orientation demonstrates early timing of compactional stabilization in calcite-cemented concretions in the Barnett Shale (Late Mississippian), Fort Worth Basin, Texas (U.S.A). Sedimentary Geology 208, 27–35.

Debacker, T.N., Hirt, A.M., Sintubin, M., Robion, P., 2009. Differences between magnetic and mineral fabrics in low-grade, cleaved siliciclastic pelites: a case study from the Anglo-Brabant deformation belt (Belgium). Tectonophysics 466, 32–46.

Delage, P., Lefebvre, G., 1984. Study of the Structure of a sensitive champlain clay and of its evolution during consolidation. Canadian Geotechnical Journal 21, 21–35.

Domnesteanu, P., McCann, C., Sothcott, J., 2002. Velocity anisotropy and attenuation of shale in under- and overpressured conditions. Geophysical Prospecting 50, 487–503.

Fawad, M., Mondol, N.H., Jahren, J., Bjorlykke, K., 2010. Microfabric and rock properties of experimentally compressed silt-clay mixtures. Marine and Petroleum Geology 27, 1698–1712.

Gale, B., Griffiths, D., 1960. Influence of instrumental aberrations on the Schulz techique for the measurement of pole figures. British Journal of Applied Physics 11, 96–102.

Haines, S.H., van der Pluijm, B.A., Ikari, M.J., Saffer, D.M., Marone, C., 2009. Clay fabric intensity in natural and artificial fault gouges: implications for brittle fault zone processes and sedimentary basin clay fabric evolution. Journal of Geophysical Research-Solid Earth 114.

Ho, N.C., Peacor, D.R., van der Pluijm, B.A., 1995. Reorientation mechanisms of phyllosilicates in the Mudstone-to-Slate transition at Lehigh Gap, Pennsylvania. Journal of Structural Geology 17, 345–356.

Ho, N.C., Peacor, D.R., van der Pluijm, B.A., 1996. Contrasting roles of detrital and authigenic phyllosilicates during slaty cleavage development. Journal of Structural Geology 18, 615–623.

Ho, N.C., Peacor, D.R., van der Pluijm, B.A., 1999. Preferred orientation of phyllosilicates in Gulf Coast mudstones and relation to the smectite-illite transition. Clays and Clay Minerals 47, 495–504.

Huijser-Gerits, E.M.C., Rieck, G.D., 1974. Defocusing effects in the reflexion technique for the determination of preferred orientation. Journal of Applied Crystallography 7, 286–290.

Jacob, G., Kisch, H.J., van der Pluijm, B.A., 2000. The relationship of phyllosilicate orientation, X-ray diffraction intensity ratios, and c/b fissility ratios in metasedimentary rocks of the Helvetic zone of the Swiss Alps and the Caledonides of Jamtland, central western Sweden. Journal of Structural Geology 22, 245–258.
Kenney, T.C., 1964. Sea-level movements and the geologic histories of the post-glacial marine soils at Boston, Nicolet, Ottawa and Oslo. Geotechnique 14, 203–230.
Kocks, U.F., Tomé, C., Wenk, H.-R., 1998. Texture and Anisotropy. Preferred Orientations in Polycrystals and Their Effect on Materials Properties. Cambridge University Press.
Loucks, R.G., Reed, R.M., Ruppel, S.C., Jarvie, D.M., 2009. Morphology, genesis, and distribution of nanometer-scale pores in siliceous mudstones of the Mississippian Barnett shale. Journal of Sedimentary Research 79, 848–861.
Lutterotti, L., Voltolini, M., Wenk, H.-R., Bandyopadhyay, K., Vanorio, T., 2009. Texture analysis of a turbostratically disordered Ca-montmorillonite. American Mineralogist 95, 98–103.
Manda, A.K., Mabee, S.B., Wise, D.U., 2008. Influence of rock fabric on fracture attribute distribution and implications for groundwater flow in the Nashoba Terrane, eastern Massachusetts. Journal of Structural Geology 30, 464–477.
Roduit, N., 2008. JMICROVISION: Image Analysis Toolbox for Measuring and Quantifying Components of High-definition Images.
Sander, B., 1930. Gefügekunde der Gesteine. Springer, Berlin.
Santagata, M.C., Kang, Y.I., 2007. Effects of geologic time on the initial stiffness of clays. Engineering Geology 89, 98–111.
Sayers, C.M., 1994. The elastic-anisotropy of shales. Journal of Geophysical Research-Solid Earth 99, 767–774.
Sayers, C.M., 1999. Stress-dependent seismic anisotropy of shales. Geophysics 64, 93–98.
Sayers, C.M., 2005. Seismic anisotropy of shales. Geophysical Prospecting 53, 667–676.
Schleicher, A.M., Warr, L.N., van der Pluijm, B.A.V., 2009. On the origin of mixed-layered clay minerals from the San Andreas Fault at 2.5–3 km vertical depth (SAFOD drillhole at Parkfield, California). Contributions to Mineralogy and Petrology 157, 173–187.
Schneider, J., Flemings, P.B., Day-Stirrat R.J., Germaine, J.T., . Insights into pore-scale controls on mudstone permeability through resedimentation experiments. Geology (in press).
Sheahan, T.C., 1991. An experimental study of the time-dependent undrained shear behavior of resedimented clay using automated stress path triaxial equipment. Department of Civil Engineering. Massachusetts Institute of Technology, Cambridge. 952.
Sintubin, M., 1994a. Clay fabrics in relation to the burial history of shales. Sedimentology 41, 1161–1169.
Sintubin, M., 1994b. Phyllosilicate preferred orientation in relation to strain Path determination in the lower Paleozoic Stavelot-Venn Massif (Ardennes, Belgium). Tectonophysics 237, 215–231.
Solum, J.G., van der Pluijm, B.A., 2009. Quantification of fabrics in clay gouge from the Carboneras fault, Spain and implications for fault behavior. Tectonophysics 475, 554–562.
Solum, J.G., van der Pluijm, B.A., Peacor, D.R., 2005. Neocrystallization, fabrics and age of clay minerals from an exposure of the Moab Fault, Utah. Journal of Structural Geology 27, 1563–1576.
Solum, J.G., van der Pluijm, B.A., Peacor, D.R., Warr, L.N., 2003. Influence of phyllosilicate mineral assemblages, fabrics, and fluids on the behavior of the Punchbowl fault, southern California. Journal of Geophysical Research-Solid Earth 108.
Tenckhoff, E., 1970. Defocusing for the Schulz technique of determining preferred orientation. Journal of Applied Physics 41, 3944–3948.
van der Pluijm, B.A., Ho, N.-C., Peacor, D.R., 1994. High-resolution X-ray texture goniometry. Journal of Structural Geology 16, 1029–1032.
Vernik, L., 2008. Anisotropic correction of sonic logs in wells with large relative dip. Geophysics 73, E1–E5.
Vernik, L., Landis, C., 1996. Elastic anisotropy of source rocks: implications for hydrocarbon generation and primary migration. Aapg Bulletin-American Association of Petroleum Geologists 80, 531–544.
Vernik, L., Liu, X.Z., 1997. Velocity anisotropy in shales: a petrophysical study. Geophysics 62, 521–532.
Voltolini, M., Wenk, H.R., Mondol, N.H., Bjorlykke, K., Jahren, J., 2009. Anisotropy of experimentally compressed kaolinite-illite-quartz mixtures. Geophysics 74, D13–D23.
Weaver, C.E., 1989. Clays, muds, and shales. Elsevier, Amsterdam, New York.
Wenk, H.-R., 1985. Measurement of pole figures. In: Wenk, H.-R. (Ed.), Preferred orientation in deformed metals and rocks; an introduction to modern texture analysis. Acad. Press, Orlando, FL, pp. 11–47.
Wenk, H.-R., Kanitpanyacharoen, W., Voltolini, M., 2010. Preferred orientation of phyllosilicates: comparison of fault gouge, shale and schist. Journal of Structural Geology 32, 478–489.
Wenk, H.-R., Voltolini, M., Kern, H., Popp, T., Mazurek, M., 2008a. Anisotropy in shale from Mont Terri 10.1190/1.2944159. The Leading Edge 27, 742–748.
Wenk, H.-R., Voltolini, M., Mazurek, M., Van Loon, L.R., Vinsot, A., 2008b. Preferred orientations and anisotropy in shales: Callovo-Oxfordian shale (France) and Opalinus clay (Switzerland). Clays and Clay Minerals 56, 285–306.
Worden, R.H., Charpentier, D., Fisher, Q.J., Aplin, A.C., 2005. Fabric development and the smectite to illite transition in Upper Cretaceous mudstones from the North Sea: an image analysis approach. In: Shaw, R.P. (Ed.), Understanding the Micro to Macro Behaviour of Rock-Fluid Systems. Geological Society, London, pp. 103–114. Special Publications.